Article

Penetration of Cell Membranes and Synthetic Lipid Bilayers by Nanoprobes

Matthew R. Angle,[1] Andrew Wang,[1] Aman Thomas,[1] Andreas T. Schaefer,[1] and Nicholas A. Melosh[1,*]
[1]Department of Materials Science and Engineering, Stanford University, Stanford, California

ABSTRACT Nanoscale devices have been proposed as tools for measuring and controlling intracellular activity by providing electrical and/or chemical access to the cytosol. Unfortunately, nanostructures with diameters of 50–500 nm do not readily penetrate the cell membrane, and rationally optimizing nanoprobes for cell penetration requires real-time characterization methods that are capable of following the process of membrane penetration with nanometer resolution. Although extensive work has examined the rupture of supported synthetic lipid bilayers, little is known about the applicability of these model systems to living cell membranes with complex lipid compositions, cytoskeletal attachment, and membrane proteins. Here, we describe atomic force microscopy (AFM) membrane penetration experiments in two parallel systems: live HEK293 cells and stacks of synthetic lipid bilayers. By using the same probes in both systems, we were able to clearly identify membrane penetration in synthetic bilayers and compare these events with putative membrane penetration events in cells. We examined membrane penetration forces for three tip geometries and 18 chemical modifications of the probe surface, and in all cases the median forces required to penetrate cellular and synthetic lipid bilayers with nanoprobes were greater than 1 nN. The penetration force was sensitive to the probe's sharpness, but not its surface chemistry, and the force did not depend on cell surface or cytoskeletal properties, with cells and lipid stacks yielding similar forces. This systematic assessment of penetration under various mechanical and chemical conditions provides insights into nanoprobe-cell interactions and informs the design of future intracellular nanoprobes.

INTRODUCTION

Many cellular studies involve the measurement and manipulation of intracellular activity, but directly accessing the cytoplasm of an intact cell remains an experimental challenge. Nanofabricated devices, including nanostraws (1–3), nanowires (4–7), nanoneedles (8–12), and nanoelectrodes (13–22), are increasingly being investigated as tools for cellular studies, but these structures do not readily insert through the cell membrane (2–5,13,23), and assessing when (or whether) penetration has occurred is difficult due to the nanoscale features of the probe-membrane interface. To design cell-penetrating nanoprobes, a systematic approach is needed to describe nanostructure-membrane interactions at relevant temporal and spatial scales, particularly the processes of nanoprobe insertion through (3,8–13,15,18,24,25) or fusion with (14,16,19,26–28) the plasma membrane.

During plasma membrane penetration, a nanoprobe traverses the 5-nm-thick lipid bilayer in <1 ms (29). Characterizing this process therefore requires a combined spatial and temporal resolution that is afforded by few techniques. Electron microscopy (EM) has sufficient spatial resolution to image membrane penetration (4,5,21), but it cannot temporally resolve the penetration process, and artifacts associated with EM sample preparation, such as changes in extracellular space and membrane breakage (30,31), complicate the interpretation of EM images of cell-nanostructure interfaces (32). Electrical measurements, by contrast, can measure fast (1 μs) processes, but they cannot resolve the nanoscale geometry of the nanoprobe-membrane interface, and multiple configurations can lead to similar recording properties. For instance, recording low-frequency changes in the transmembrane potential can indicate direct cytosolic access (13,17), but such changes are also observable using extracellular recordings by metal microelectrodes (33,34) or patch pipettes (35) that have sealed very tightly to the cell membrane.

Mechanical measurements using atomic force microscopy (AFM) can directly detect nanoprobe penetration through lipid membranes with microsecond, subnanometer resolution and have the advantage of reporting not only the occurrence of membrane penetration but also the mechanical force preceding it (36). AFM has been used to study the penetration of synthetic lipid bilayers (26–28,36–45) and live cells (9–12,24,29,46,47) by nanoprobes, but the reported membrane penetration forces range from <1 nN to >20 nN (12,29), and the variety of probe types, lipids, and other experimental variables make comparisons across studies difficult.

The physics of membrane penetration by AFM nanoprobes has been much more extensively studied in synthetic lipid systems (reviewed in Butt et al. (36)) than in live cells.

Submitted July 2, 2014, and accepted for publication September 16, 2014.

*Correspondence: nmelosh@stanford.edu

Matthew R. Angle and Andrew Wang contributed equally to this work.

Nicholas A. Melosh's present address is Geballe Laboratory for Advanced Materials, Stanford University, Stanford, California.

Editor: Andreas Engel.

0006-3495/14/11/2091/10 $2.00

http://dx.doi.org/10.1016/j.bpj.2014.09.023

One reason for this is the additional difficulty of interpreting AFM measurements in cells: whereas synthetic lipid systems contain only laminar lipid structures, cellular architecture includes additional structural components that can move, stretch, and break under force. To perform rigorous cell-penetration studies, therefore, it is critical to establish consistent criteria to distinguish membrane penetration events from other force-relaxation events that may occur while a cell is being indented. Comparing results between synthetic and cellular penetration experiments would provide the best criteria, but previous experiments in these two disparate systems have too many other experimental variables to allow for direct comparisons.

To enable direct comparisons between systems, we performed a series of AFM measurements in which each individual probe was tested on both live cells and stacks of tens to hundreds of synthetic lipid bilayers. In lipid stacks, which have been described elsewhere (26–28,48), neighboring lipid bilayers are spaced only by aqueous buffer, so they more closely resemble suspended lipid bilayers than do solid-supported lipid bilayers. To separate lipid bilayer penetration from other force-relaxation events, we used the breakthrough signatures in synthetic lipid stacks as a template for detecting penetration events in cells. Because synthetic and cellular bilayers differ considerably in their structure and composition, we also chose an intermediate system for comparison: cells whose cytoskeleton was chemically disrupted by cytochalasin D (10). Such cells have intact cell surfaces and native membrane composition, but no underlying cortical cytoskeleton to provide rigidity to the plasma membrane.

In these three lipid systems, we assessed the role of two factors that are thought to be important for membrane penetration: tip geometry (3,11,23) and surface chemistry (13,25,27,43). We assessed the role of nanoprobe geometry in lipid membrane penetration by using three types of nanoprobes: slender nanoneedles (11) (Fig. 1 *a*), sharp pyramids (29) (Fig. 1 *b*), and flat pyramids (Fig. 1 *c*). The nanoneedle geometry was selected based on work by Miyake and colleagues (8–12), who used the probes for cellular studies, but not in synthetic lipid bilayers. The sharp pyramids were similar to those used previously in both cell-penetration experiments (24,29) and synthetic bilayer experiments (36–44). The flat pyramids were chosen for direct comparison with the sharp pyramids to assess the importance of probe sharpness. Previous studies in supported lipid bilayers found that hydrophobic tips penetrate at lower forces than do hydrophilic ones (43). Metal nanoelectrodes (13) and micropipettes (25) also penetrate lipid bilayers more readily after hydrophobic modification. To further assess the role of probe surface chemistry in membrane penetration, we selected 18 different molecules with a range of different chemical properties and attached them to the nanoprobes by gold-thiol chemistry. These probes were also used to penetrate lipid stacks and live cells. Notably, in this screen,

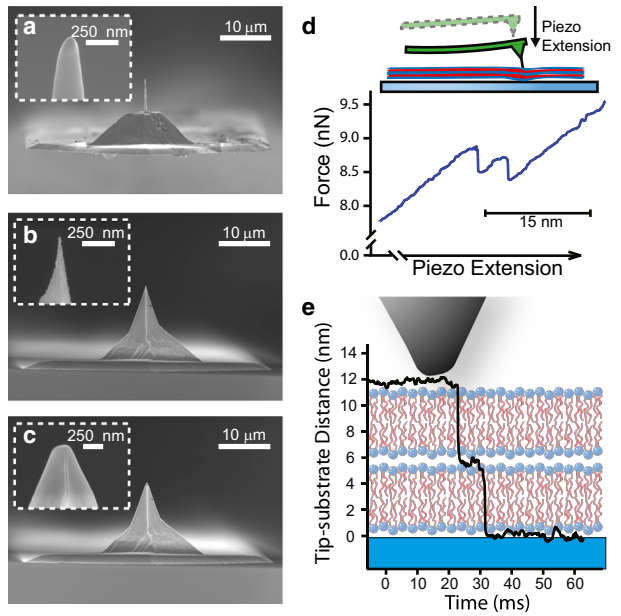

FIGURE 1 Scanning electron micrographs showing the three tip geometries of AFM cantilever tips: (*a*) nanoneedle tip, (*b*) sharp pyramidal tip, and (*c*) flat pyramidal tip. (*d*) After contact with the sample, further piezo extension results in the deflection of the cantilever and the application of force through the cantilever tip to the sample. Membrane penetration results in force relaxation. (*e*) During membrane penetration, the tip advances toward the glass substrate by the thickness of the membrane (~5 nm). A schematic lipid bilayer indicates the thickness of the compressed membranes. To see this figure in color, go online.

we selected several peptides for their known interactions with the membrane, including several cell-penetrating peptides (49–52) and pore-forming peptides (53–55). Testing the effects of geometry and surface chemistry in parallel synthetic and cellular systems further allowed us to infer which effects were specific to the lipid bilayer and which were specific to interactions with other cellular components.

MATERIALS AND METHODS

Chemicals

All chemicals, including cytochalasin D and small-molecule functionalization compounds, were purchased from Sigma-Aldrich (St. Louis, MO) unless otherwise noted. POPC was purchased from Avanti Polar Lipids (Alabaster, AL). Benzophenone silane was synthesized as follows: benzophenone-4-carboxylic acid and dicyclohexylcarbodiimide were reacted to form the corresponding anhydride, followed by thermal reaction with cysteamine, yielding C6H5-CO-C6H4-CO-NH-CH2-CH2-SH. Peptides were synthesized by Genscript USA (Piscataway, NJ). Details of the 18 molecules used for functionalization can be found in Table S1 of the Supporting Material.

Nanoprobe fabrication and chemical functionalization

Contact-mode silicon SHOCON AFM tips with spring constants k = 0.1–1 N/m were purchased from AppNano (Mountain View, CA). Tips with three different shapes (nanoneedle, sharp pyramid, and flat pyramid) were used. For nanoneedle-shaped tips, the original pyramidal tip was

milled by a focused ion beam (FIB) system (Helios NanoLab 600i; FEI, Hillsboro, OR) to a needle shape of ~10 μm in height with a spherical tip of 50–150 nm radius and base of ~1 μm radius. For sharp-pyramid-shaped tips, the original tip out of the package was used directly without modification by FIB. For flat-pyramid-shaped tips, the sharp tip apex was cut off from the side using FIB to leave a flat tip of ~150 nm radius.

To generate the Au surface for chemical functionalization, all tips were metalized with 5 nm Cr and 5–10 nm Au using sputter coating (custom-built system; Stanford Nanofabrication Facility). Before functionalization, the tips were first cleaned by oxygen plasma (Structure Probe) for 5–10 min to remove carbonaceous contamination. Small-molecule functionalization solutions were prepared in pure ethanol, and peptides were prepared in 95% ethanol/5% DMSO (% by volume). Some peptides were cofunctionalized with mercaptopropanol as a competitor to lower the surface density (see Table S1). For each treatment, three to five tips were submerged in the same chemical solution and incubated overnight. The functionalized tips were rinsed with pure ethanol, dried, and kept in air until use. All tips were used in the AFM experiments within 3 days of functionalization (storage at 20°C), generally within 6 h. All functionalization reagents were verified to form monolayers on gold by either XPS or contact angle measurements on macroscopic gold substrates.

Lipid stack and cell samples

To prepare the lipid stacks, a drop of 90% 1-palmitoyl-2-oleoyl-*sn*-glycero-3-phosphocholine (POPC)/10% cholesterol (% by weight) dissolved in chloroform at ~1 mg/mL was dried on a cleaned glass coverslip by a jet of nitrogen and left overnight under vacuum. The lipids were then smeared and thinned by a Teflon spatula and rehydrated in PBS for 2–4 h before use. Human embryonic kidney 293 (HEK293) cells were cultured in Dulbecco's modified Eagle's medium (DMEM) with 5% CO_2 at 37°C until they were 50–80% confluent. Cytochalasin D-treated cells were incubated with 17 μM of cytochalasin D (8.3 μg/ml) at room temperature for at least 20 min before measurement. For all experiments, the live cells were measured in their original culture media at room temperature for <2 h.

Force-testing experiments in AFM

Experiments were performed on an atomic force microscope (MFP-3D; Asylum Research, Santa Barbara, CA) set up on an inverted optical microscope. The spring constants and optical sensitivities of the AFM tips were calibrated in situ in the same medium as the sample using a thermal method (56). An AFM tip was positioned above a target cell or stack as confirmed by the optical microscope. In each force-testing experiment, the tip was moved by extension of the Z-piezo scanner at a rate of 300 nm/s. The force was loaded up onto the sample as the tip advanced. This force relaxed transiently when a penetration occurred (Fig. 1 *d*) or when some other structural frustration was overcome. Penetration events corresponded to advancements of the tip toward the substrate in discrete steps of ~5 nm (Fig. 1 *e*). More rarely, the two leaflets of the bilayer failed separately and could be distinguished as two successive ~2.5 nm events. The tip eventually penetrated through the whole sample and arrived at the glass substrate underneath the sample. The force continued to increase as the tip pushed against the substrate until a predetermined force limit was reached and the tip was retracted from the sample. Force (spring constant × cantilever deflection) and Z-piezo scanner extension were acquired at 50 kHz for all experiments and low-pass filtered to 1 kHz for display in figures. For each tip, three to 10 force-testing experiments were repeated on both cells and lipid stacks. Experiments could be repeatedly performed on the same stack without changing the X-Y position and yielded indistinguishable results, implying that the lamellae quickly resealed following complete tip retraction. Cell penetration was performed on each cell only once, meaning that each tip penetrated at least three different cells. Upon retraction from the stack or cell, membrane tethers were often observed for all probe types regardless of geometry or surface chemistry. These tethers were always broken before resuming experiments.

Data analysis and statistics

Penetration events were automatically detected and manually confirmed using custom analysis procedures developed in Igor Pro 6.32 (Wavemetrics Portland, OR). To test the statistical differences in penetration forces, we looked at the logarithmic distribution of all the forces of first breakthrough for each sample. When two distributions were lognormally distributed (Lilliefors test, $p > 0.1$ (57)), they were compared by Student's *t*-test. Otherwise, the Kolmogorov-Smirnov (KS) test (57), which compares the cumulative probability distributions and is sensitive to differences in both the mean and shape of the two distributions, was used. For the specific case of the nanoneedle tips, where the same eight tips were used in three different lipid types, pairwise percentage differences were computed for the median breakthrough forces of a given tip in the three samples (synthetic lipid stacks, cytochalasin D-treated cells, and untreated cells). These pairwise differences ($n = 8$ for each) were normally distributed (Lilliefors test, $p > 0.1$) and were appropriately compared using a paired *t*-test.

RESULTS

In our first set of experiments, we evaluated membrane penetration by nanoneedle-shaped probes. Standard contact-mode AFM tips were modified by FIB milling (11) to adopt the shape of a slender nanoneedle with a tip apex of ~300 nm in diameter (Fig. 1 *a*). After FIB milling, these tips were then mounted onto a piezo-controlled AFM stage located above a petri dish containing either lipid bilayer stacks (Fig. 2) or live HEK293 cells (Fig. 3).

To confidently define the criteria for membrane-penetration events, we performed experiments in stacks of synthetic lipid bilayers (Fig. 2), which were formed by hydrating a cake of dried lipid in PBS (26–28). This preparation resulted in stacks of uniformly spaced bilayers that were tens to hundreds of micrometers in diameter and ~200 bilayers thick, with stack thickness having no effect on penetration force (see Fig. S1 in the Supporting Material for details on lipid stacks).

We inserted the nanoprobe into the lipid stacks by advancing the Z-piezo scanner at a constant speed and retracted it when it reached a predetermined force limit, which was set sufficiently high ($\geq$80 nN) to ensure that all membranes under the tip were ruptured before the experiment was ended. The cantilever deflection (proportional to the force applied to the lipid membrane) and tip position relative to the glass substrate were acquired and analyzed to determine when a membrane penetration had occurred. As previously reported in studies using lipid stacks (26–28), membrane penetration appeared as discrete advances in tip position relative to the substrate of either 5 nm (the thickness of a single bilayer) or multiples of 5 nm, which we interpret to be rapid successive membrane breakthroughs (Fig. 2 *a*). This was accompanied by a relaxation of cantilever deflection/force (Fig. 2 *b*). Importantly, the only structural features available to rupture in this system were the

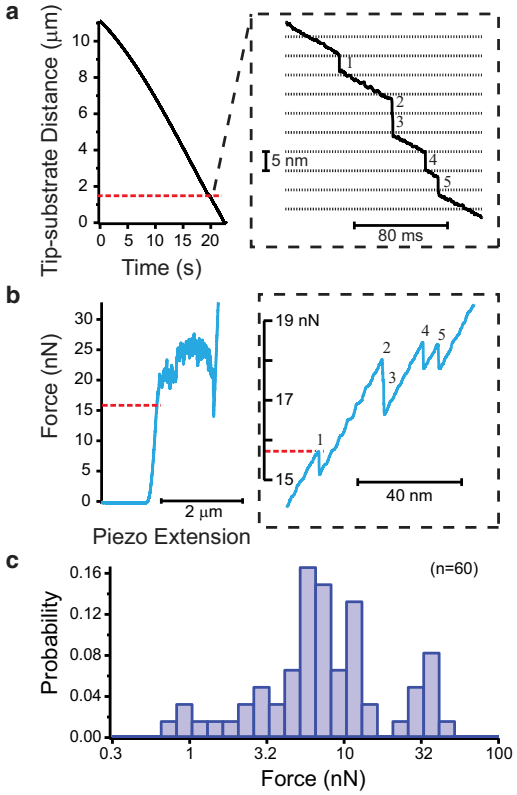

FIGURE 2 Lipid bilayer stack penetration. (*a*) Representative plot of the tip movement toward the glass substrate as the lipid stack compresses and is penetrated (first penetration indicated by a *red line*). Zoom: during penetration, the tip advances 5 nm, the distance of a single bilayer. The tip movement that occurs between penetration events is compression of the entire stack. The inset shows only five of the hundreds of penetration events that occurred in this experiment. (*b*) Force applied to the sample. As the Z-piezo scanner extends, it pushes the cantilever forward. When the tip encounters the substrate, it begins to deflect, and force mounts on the sample. Membrane penetration relaxes the force on the cantilever, causing a saw-tooth deflection signal as hundreds of membranes are penetrated. Zoom: the same five breakthrough events shown in panel a. The red line indicating first penetration also shows the force at which penetration has occurred. (*c*) Probability histogram of the force of first breakthrough ($n = 60$). To see this figure in color, go online.

membrane lamellae themselves, which allowed us to attribute discrete jumps in tip position to lipid bilayer ruptures.

We repeated this experiment using eight different nanoneedle-shaped probes, for a total of 60 experiments. For each experiment, the force observed just before the rupture of the topmost bilayer in the stack was noted. The force preceding the first penetration event was deemed particularly important because in cellular studies the first membrane penetration provides access to the cytoplasm. To make the comparison most direct, only the first penetration event in the lipid stacks was used to calculate the penetration force, although a comparison of the first and second breakthroughs in all stacks revealed no difference between the topmost bilayer and the one directly underlying it (Fig S1). Pooling all 60 experiments yielded a median force of the first penetration equal to 6.7 nN, with the first (Q1) and third (Q3) quartiles being 4.3 nN and 11.4 nN, respectively. A histogram of all first penetration forces in lipid stacks is shown in Fig. 2 *c*.

After observing unambiguous membrane-penetration events in the synthetic system, we next performed the same penetration experiments in live HEK293 cells, using the same set of probes previously used on the stacks (Fig. 3). HEK293 cells were specifically chosen for comparability with previous studies (10,11). We observed that during indentation, the cells were so compliant that they were easily compressed with <1 nN of applied force. The compression leading up to the first penetration event apparently expelled most of the cytoplasmic material from the area of the cell directly underneath the probe, because by the time of penetration, the distance between the tip and glass substrate was roughly the combined thickness of the compacted bilayers (Fig. 3). We interpret this to mean that the cytoskeletal elements and smaller organelles can be pushed away from the tip during indentation, resulting in a tightly packed stack of membranes that is similar to the synthetic lipid stacks. The first penetration event was recognizable as an abrupt 5 nm probe advancement and occurred when the applied force reached roughly 10 nN (median: 11.2 nN; Q1: 8.3 nN; Q3: 21.7 nN; $n = 87$). After the first penetration event, subsequent penetrations often occurred in rapid succession, leading to tip displacements occurring in clear multiples of 5 nm (Fig. 3).

To assess the influence of the actin cytoskeleton, which was found by others to be necessary for membrane penetration at low force (10), we also performed the same penetration experiments using the same eight probes on HEK cells whose cytoskeletons were disrupted by treatment with cytochalasin D. We found that the penetration forces were similar to the untreated cells (median: 11.6 nN; Q1: 6.8 nN; Q3: 20.3 nN; $n = 63$). A histogram of all first penetration forces for both untreated and treated cells is shown in Fig. 4 *a*.

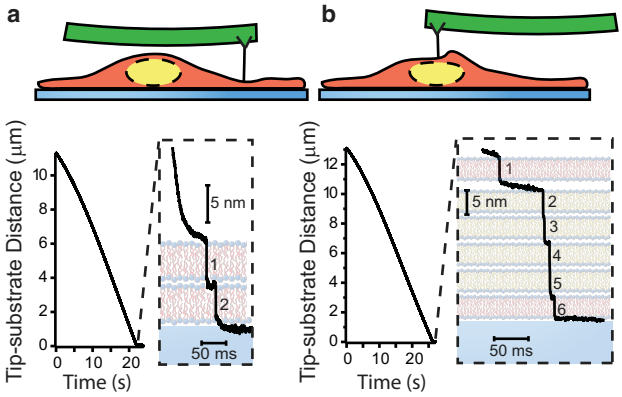

FIGURE 3 Cell membrane penetration. Representative plots of the tip movement toward the glass substrate when the tip was above the periphery (*a*) or the nucleus (*b*) of an untreated cell. Zoom-ins show two and six penetration events, respectively. To see this figure in color, go online.

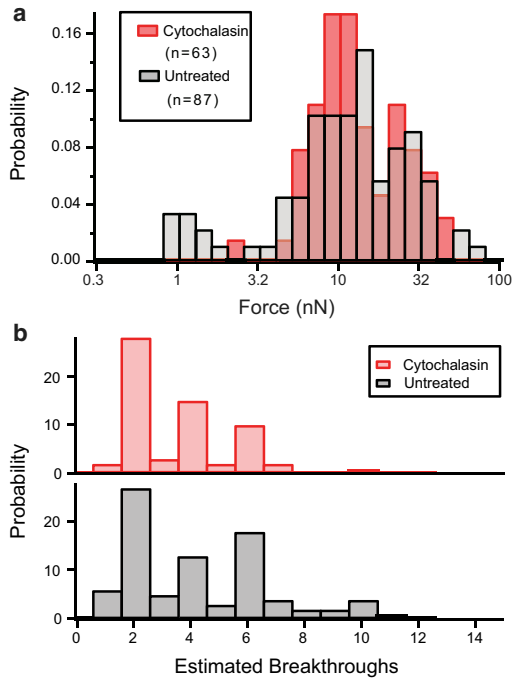

FIGURE 4 Characterization of cell membrane penetration with and without the presence of actin cytoskeleton. (*a*) Probability histogram of the force of first breakthrough in untreated HEK cells ($n = 87$) and in cytochalasin D-treated HEK cells ($n = 63$). (*b*) Probability histogram of the total breakthrough number for untreated and cytochalasin D-treated HEK cells. To see this figure in color, go online.

Given the complexity of cells, we looked for a way to verify that we were correctly detecting penetration events. Since cellular membranes are closed lipid systems, we know that when a cell is compressed between the probe and glass substrate, the resulting stack of lipid bilayers will have a number of lamellae that is twice the number of intact membranes. In this arrangement, after the cell is completely penetrated and the tip is in contact with the glass substrate, the pinned bilayers should fail independently and the number of detected penetrations should be equal to the number of lamellae. We largely confirmed this assumption by counting the total number of 5-nm-advancement events in cells (Fig. 4 *b*). We found a much higher probability of even-numbered events: 86% and 75% of experiments had an even number of events in treated and untreated cells, respectively, excluding two experiments in which multiple cells were penetrated (i.e., more than 12 breakthroughs occurred). Interestingly, experiments performed at the center of the cell often resulted in six membrane-penetration events, as compared with only two events on the periphery of the cell, with the four additional events suggesting penetration of the double-membrane structure of the nuclear membrane.

We can propose two possible interpretations for experiments with odd numbers of events: 1), early retraction of nanoprobes before all lipid membranes were penetrated; and/or 2), undetected low-force penetration events in the regime of <1 nN. Therefore, we closely examined the force-displacement curve for each experiment, noting any sudden deviations from smooth deformation, and then looked at the corresponding record of the tip trajectory as a function of time. We found that events that occurred at forces of <1 nN did not resemble penetration events observed on lipid stacks or in high-force regimes in cells, in that they had slow dynamics and often short distances of probe advancement (Fig. 5). These events were commonly found in cases where the number of unambiguous membrane breakthroughs was already even, as in Fig. 5, and they were more prevalent in untreated cells, suggesting that such events were cytoskeletal in origin.

To further assess the differences in penetration force among the three lipid systems, we employed two statistical analyses. First, to properly treat probe-to-probe variations, we compared the median penetration forces of different lipid systems measured by the same nanoprobe pairwise (i.e., untreated versus treated cells, untreated cells versus stacks, and treated cells versus stacks). For each probe, the relative difference between median penetration forces was calculated using Eq. 1:

$$\%\ \textit{difference} = \left(\frac{\overline{F}_A - \overline{F}_B}{\overline{F}_A + \overline{F}_B}\right) \times 100\% \qquad (1)$$

where *A* and *B* refer to any two of the three lipid systems. Paired *t*-tests of the relative differences of all eight probes revealed no significant difference among different lipid

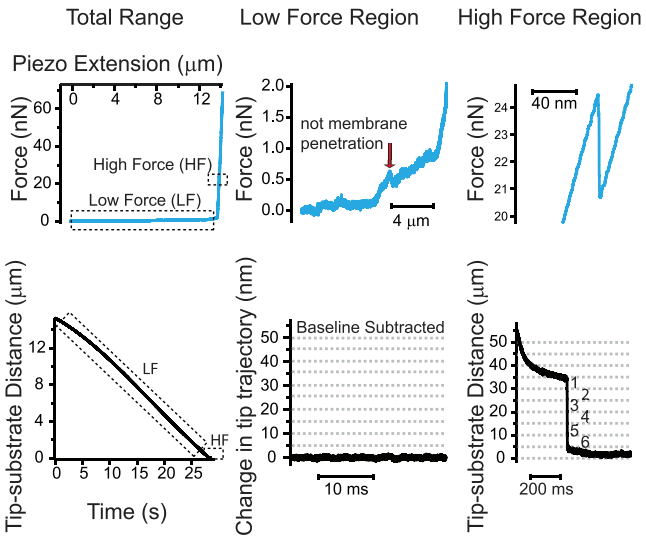

FIGURE 5 Force relaxation events and corresponding change in tip position in low- and high-force regimes. Top row: force curve for a representative penetration experiment in an untreated HEK cell. Bottom row: corresponding tip movement relative to glass. Middle column: low-force region showing several small force relaxation events with little change in tip position (baseline tip trajectory subtracted for display). Right column: high-force region showing six 5 nm penetration events for a total of 30 nm tip displacement. To see this figure in color, go online.

systems ($p > 0.05$ for all cases; Fig. 6 *a*). For the second analysis, we adopted the nonparametric KS test (57) to compare the overall distribution of penetration forces on different lipid systems pooled from all eight probes (Fig. 6 *b*). Since the KS test was sensitive to the profile of the distribution in addition to the central value, it showed that the distribution of breakthrough forces for the stacks was significantly different from that of either the untreated or treated cells ($p = 0.0024$ and 0.0002, respectively).

The similar median penetration forces across systems suggest that the lipid bilayer itself is the key structural element that must be disrupted for cell penetration, since the forces are not sensitive to the exact membrane composition, presence of extracellular glycoproteins, or underlying actin cytoskeletal structure. However, subtle differences between stacks and cells as detected by the KS test suggest that composition variation may still play some secondary role in membrane penetration.

After specifically investigating the membrane penetration force for high-aspect-ratio nanoneedles, we next sought to determine the importance of two factors in penetration forces: probe sharpness (Fig. 7) and surface chemistry (Fig. 8). Given the previous observation that treated and untreated cells behaved identically, to reduce the number of nonpenetration events in cells and thus simplify our analysis, we conducted all of the remaining experiments in cytochalasin D-treated cells and lipid bilayers. To assess the

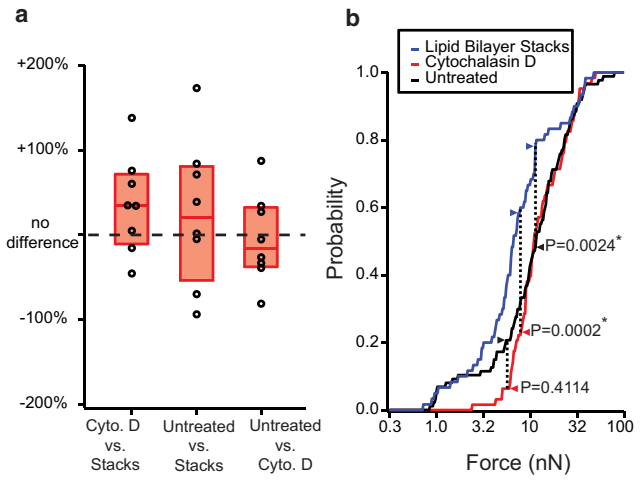

FIGURE 6 Comparing breakthrough forces between bilayer types. (*a*) Pairwise differences between median breakthrough forces in stacks, untreated HEK cells, and cytochalasin D-treated HEK cells. Each point represents the median breakthrough force from all experiments done with a different nanoneedle probe. Boxplots represent median and quartiles of median breakthrough forces from the eight probes. No significant difference was found by paired *t*-test between the mean of medians for any two bilayer types. (*b*) Cumulative probability histogram for all breakthrough forces and KS test. The untreated and cytochalasin D-treated cells are statistically indistinguishable from one another (Ne = 35.6, D = 0.1434, $p = 0.41$). The lipid stacks differed from both the untreated cells (Ne = 35.5, D = 0.3778, $p = 0.0024$) and treated cells (Ne = 30.7, D = 0.3006, $p = 0.0002$). To see this figure in color, go online.

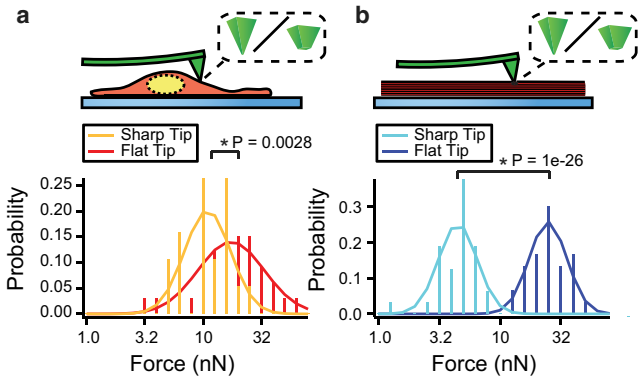

FIGURE 7 Effect of tip geometry on penetration force. (*a*) Probability histogram of first breakthrough forces in cells for flat and sharp tips. (*b*) Probability histogram of first breakthrough forces in lipid bilayer stacks for flat and sharp tips. To see this figure in color, go online.

effect of probe sharpness, we performed penetration experiments using unmodified pyramidal AFM tips with a tip diameter of <25 nm (Fig. 1 *b*, referred to as sharp tip) and FIB-flattened tips with a 300 nm tip diameter (Fig. 1 *c*, flat tip). In these experiments, tip surface properties were also controlled by chemical functionalization with a hydrophilic thiol (mercaptopropanol), which was used to prevent nonspecific adsorption of material to the probe surface. The five flat tips had a significantly higher median breakthrough force than the four sharp tips in both cells and stacks ($p < 0.005$, unpaired *t*-test). In cells (Fig. 7 *a*), the flat tips had a median force of first penetration of 21.2 nN ($n = 33$), whereas the median for sharp tips was 11.8 nN ($n = 19$). In lipid stacks (Fig. 7 *b*), the median force was 27.2 nN for flat tips ($n = 30$) and 5.21 nN ($n = 32$) for sharp tips. Although sharp nanoprobes penetrated more easily than flat-tipped probes, none of the tips tested were able to penetrate membranes with <1 nN applied force. This magnitude has some relevance to nanowire arrays, suggesting that the forces of cellular adhesion alone are unlikely to result in spontaneous penetration by similarly sized nanostructures (23).

Finally, to test the role of probe surface chemistry in membrane penetration, we compared the penetration forces on treated cells and lipid stacks by a set of probes with controlled geometry (FIB-milled, flat, 300 nm diameter) and different chemical functionalization. Use of the FIB allowed for more reproducible tip shapes compared with those supplied commercially, thus minimizing variability in penetration force not due to surface chemistry. The 300 nm diameter is also comparable in size to several nanoprobes used in cellular studies (1,4,13,17,21). Eighteen molecules, ranging from hydrophilic to hydrophobic and including several known membrane-interacting peptides, such as melittin (54), TAT (51), penetratin (50), and MAP (52), were used. As summarized in Fig. 8, the treatments were ordered (increasing from top to bottom) by their median forces in cytochalasin D-treated cells. Surprisingly,

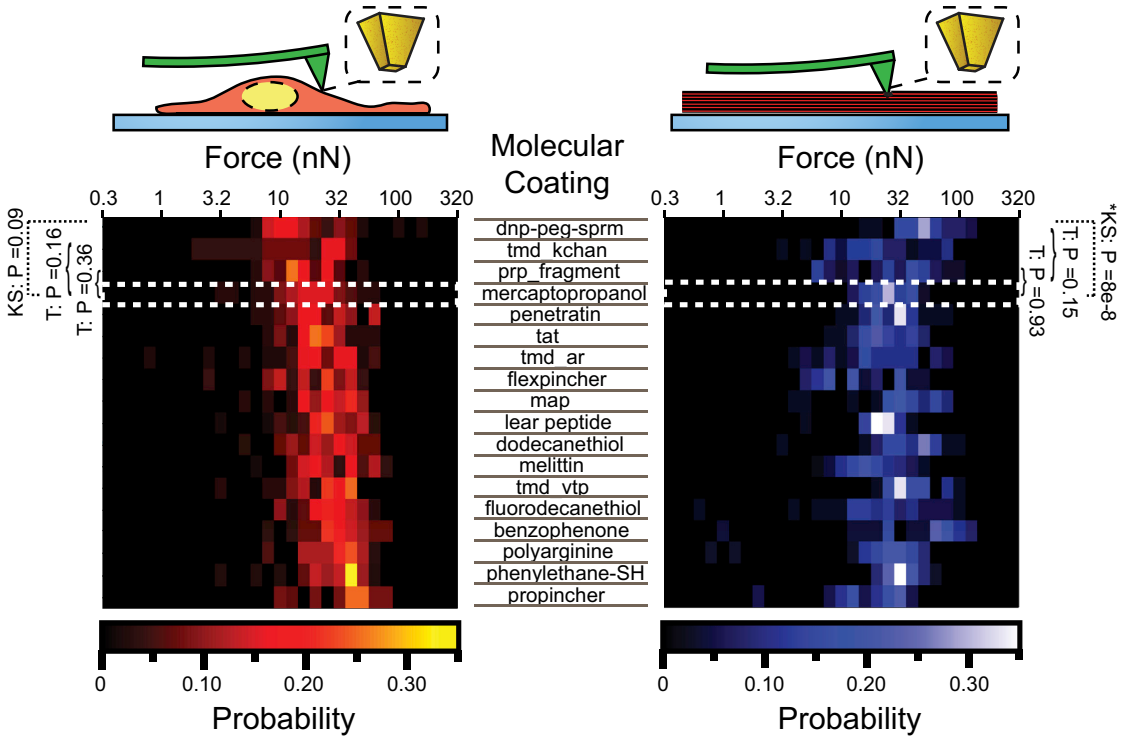

FIGURE 8 Effect of surface functionalization on penetration force. Left: combined histogram of first breakthrough force for all surface functionalizations, ranked from top to bottom in increasing median force. The white dotted box indicates mercaptopropanol control. Brackets on the margin denote unpaired *t*-test (T) and the black dotted line indicates the KS test. Right: corresponding histogram for lipid bilayer stacks. To see this figure in color, go online.

we observed no obvious correlation between hydrophobicity and membrane-penetration force, and none of the membrane-interacting peptide sequences (49–55,58) had a discernible effect on membrane-penetration force. No treatments resulted in a median cell-penetration force that was statistically significantly different from the hydrophilic control, mercaptoethanol ($p > 0.05$, KS test). The only molecule that showed different behavior from the others was a synthetic oligomer with alternating hydrophobic and cationic stretches (dinitrophenol-polyethyleneglycol-spermine; see Fig. S2 in the Supporting Material). Its median breakthrough force ranked lowest on cells (14 nN) but was relatively high in stacks (56 nN), where it differed significantly from the mercaptopropanol control (KS test, $p = 8 \times 10^{-8}$). In all, surface chemistry seemed to have little influence on the penetration forces of flat tips. Whether these chemical modifications could lower penetration forces for probes of other geometries or whether specific patterning of the functionalization would affect penetration forces remains a topic for further investigations.

DISCUSSION

In this work, we performed paired AFM membrane-penetration experiments in synthetic lipid bilayer stacks and live cells. A key finding of this combined study is the confirmation that the AFM signature for lipid bilayer rupture is exactly the same in both systems, appearing as discrete events in which the probe advances in multiples of 5 nm. Further, the median breakthrough forces in synthetic and cellular membranes are largely the same (5–20 nN) across a wide range of tip conditions. This result is a strong indicator that the limiting factor for probe insertion into a cell is the rupture of the lipid bilayer itself, and not any other cell-specific component of the membrane (i.e., cortical cytoskeleton or glycocalyx).

We specifically tested the hypothesis that the force required to penetrate the plasma membrane with nanoprobes is affected by the presence of the actin cytoskeleton. We found no evidence of such an effect, with cytochalasin D-treated HEK cells being statistically indistinguishable from untreated HEK cells. This result seemingly differs from a report by Kagiwada et al. (10), who found that cytochalasin D-treated cells and liposomes were more difficult to penetrate than untreated cells. It should be noted that in that study, the authors stopped the penetration experiment at low force after indenting the membrane only slightly, instead of increasing the force to see at what point penetration would have occurred. We have found that live cells tend to compress without membrane rupture until they reach a point where all nonmembranous material has been expelled from the region under the tip and the cell is only tens of nanometers thick.

The lack of membrane penetration in liposomes and cytochalasin D-treated cells in the study by Kagiwada et al. (10)

is explained by the high forces we measured for membrane penetration. However, the observations by several groups (9–12) of membrane penetration in untreated cells at sub-nano-Newton forces are more difficult to reconcile with our results. One possibility, given the similarity between previously published penetration events (11,12) and some of the demonstrable nonpenetration events in our data set (Fig. 4), is that a portion of the low-force penetrations reported elsewhere are in fact not membrane-related. These small cantilever deflections may be caused by cytoskeletal failures, consistent with their reported disappearance after cytochalasin D treatment and the fact that they are never observed in liposomes (10). Other independent evidence for low-force penetration, namely, molecular delivery (8,9), supports the interpretation that low-force cantilever deflections represent bona fide membrane penetrations, but this indirect evidence must be tempered by recent findings suggesting that molecular delivery by nanowires may be penetration independent (4,5).

The forces we report for live-cell membrane penetration by sharp pyramidal tips are comparable to those reported by Hategan et al. (29) and Guillaume-Gentil et al. (24), who confirmed penetration of the plasma membrane and nuclear envelope by fluidic delivery of molecules to the nucleus using a hollow AFM tip. The penetration forces we report for flat tips in lipid bilayer stacks are also consistent with other studies performed in lipid bilayer stacks using similar structures (26–28). Not surprisingly, our results indicate that the force required to penetrate cells with sharp nanoprobes (<25 nm diameter) is lower than that required for flat-tip probes. Since penetration is caused by local pressure and not total force, it follows that sharper probes should enter the cell at lower force, as they apply greater pressure for the same applied force. Moreover, probes with a diameter of <100 nm can introduce significant bending energy into the contacted lipid bilayer, which also increases the likelihood of penetration (23). Our results agree with this assumption, but the difference in penetration force is not as great as one might expect by simply comparing the differences in area between the sharp and flat probes, which would predict a ~100-fold pressure difference. We observe only a 2- to 5-fold change in breakthrough force, which may be attributable to the fact that the faces of the flat tips are not perfectly parallel to the glass during compression. This could result in edge-on contact with the lipid bilayer, where the radius of curvature is ~50 nm for most tips.

Finally, because we and others previously found that the chemistry of the probe surface plays an important role in modulating its interactions with the lipid membranes (13,25,27,43), we had hypothesized that the membrane penetration force would be affected by probe surface chemistry. Instead, we found that the membrane was equally resilient to both hydrophilic and hydrophobic surfaces, and that none of the 18 chemical functionalizations we tested were able to lower the breakthrough force in cells or stacks. Surprisingly, we found that none of the membrane-inserting peptides or peptides derived from protein transmembrane domains could sufficiently destabilize the membrane to allow for lower-force penetration. One possible explanation for the lack of variability between probe treatments despite the very different chemical properties is that the probe tip may quickly become coated in lipids, as was hypothesized in previous studies involving AFM experiments in supported lipid bilayers (59). We did not observe a change in penetration force over the course of successive penetrations, but we cannot exclude the possibility that the tip surface becomes coated by free lipid or other biological molecules before the first penetration.

Another possible caveat to the chemical functionalization experiments is that they were performed at a fixed rate of piezo extension (300 nm/s) rather than a fixed force-loading rate, and the cell membranes were usually compressed with very little space between them before membrane failure occurred. This means that the force-loading rate was often very high at the time of penetration (30–150 nN/s). It is possible that some lipid rearrangements, peptide conformational changes, and other processes that would ultimately lower the energy barrier to membrane failure occur at a rate that is slow relative to this loading rate. To fully investigate the potential of chemical functionalization to facilitate membrane penetration, it will be necessary to probe longer timescales (i.e., slower loading rates), which would allow for more dramatic molecular reorganization at the nanoprobe-lipid interface. Extending our current experimental design to different loading rates (40,45) should also allow us to explore the energetics of membrane penetration and predict the failure rates under very small static forces, such as those experienced by cells growing on a nanowire array (2).

CONCLUSIONS

We have confirmed that membrane penetration is highly comparable between synthetic lipid bilayers and live cells, and that the forces required to achieve membrane penetration range from 5 to 20 nN depending on the sharpness of the probe. In cells, this force is not appreciably influenced by the actin cytoskeleton. These findings suggest that nanoprobe penetration of lipid membranes is remarkably insensitive to membrane composition and cellular components. We also note that cell penetration by nanoprobes requires an amount of applied force that is large relative to cellular forces (23). Based on recent findings by Hanson et al. (4) and Mumm et al. (5) that nanowires rarely (if ever) spontaneously penetrate cells, and our own findings regarding the low probability of nanostraw penetration (3), a consensus is beginning to emerge that simply making a probe nanoscale will not ensure its easy insertion into the plasma membrane. Nor, for that matter, would any of the

18 different, widely varying chemical functionalizations we tested, which surprisingly had no effect on membrane-penetration force in cells. Therefore, future intracellular devices in the size range of 25–250 nm will need to be designed to interact more specifically with the cell membrane if they are to achieve low-force entry into cells.

SUPPORTING MATERIAL

Two figures, and one table are available at http://www.biophysj.org/biophysj/supplemental/S0006-3495(14)00997-7.

The authors acknowledge Herbert Zimmermann (Max Planck Institute for Medical Research) for synthesizing benzophenone silane, Katie Chang for help with cantilever preparation, and Nate Hohman and Alex Xu for suggestions on the manuscript. This work was supported by Stanford Neuroventures, the National Science Foundation (NSF IDBR-1063397), the Human Frontiers Science Program (program grant to N.M. and A.T.S.), and the Max Planck Society (A.T.S. and M.R.A.).

REFERENCES

1. VanDersarl, J. J., A. M. Xu, and N. A. Melosh. 2012. Nanostraws for direct fluidic intracellular access. *Nano Lett.* 12:3881–3886.
2. Xie, X., A. M. Xu, …, N. A. Melosh. 2013. Nanostraw-electroporation system for highly efficient intracellular delivery and transfection. *ACS Nano.* 7:4351–4358.
3. Xu, A. M., A. Aalipour, …, N. A. Melosh. 2014. Quantification of nanowire penetration into living cells. *Nat. Commun.* 5:3613.
4. Hanson, L., Z. C. Lin, …, B. Cui. 2012. Characterization of the cell-nanopillar interface by transmission electron microscopy. *Nano Lett.* 12:5815–5820.
5. Mumm, F., K. M. Beckwith, …, P. Sikorski. 2013. A transparent nanowire-based cell impalement device suitable for detailed cell-nanowire interaction studies. *Small.* 9:263–272.
6. Shalek, A. K., J. T. Robinson, …, H. Park. 2010. Vertical silicon nanowires as a universal platform for delivering biomolecules into living cells. *Proc. Natl. Acad. Sci. USA.* 107:1870–1875.
7. Bonde, S., N. Buch-Månson, …, K. L. Martinez. 2014. Exploring arrays of vertical one-dimensional nanostructures for cellular investigations. *Nanotechnology.* 25:362001.
8. Han, S., C. Nakamura, …, J. Miyake. 2005. Gene expression using an ultrathin needle enabling accurate displacement and low invasiveness. *Biochem. Biophys. Res. Commun.* 332:633–639.
9. Han, S. W., C. Nakamura, …, J. Miyake. 2005. A molecular delivery system by using AFM and nanoneedle. *Biosens. Bioelectron.* 20: 2120–2125.
10. Kagiwada, H., C. Nakamura, …, J. Miyake. 2010. The mechanical properties of a cell, as determined by its actin cytoskeleton, are important for nanoneedle insertion into a living cell. *Cytoskeleton (Hoboken).* 67:496–503.
11. Obataya, I., C. Nakamura, …, J. Miyake. 2005. Nanoscale operation of a living cell using an atomic force microscope with a nanoneedle. *Nano Lett.* 5:27–30.
12. Obataya, I., C. Nakamura, …, J. Miyake. 2005. Mechanical sensing of the penetration of various nanoneedles into a living cell using atomic force microscopy. *Biosens. Bioelectron.* 20:1652–1655.
13. Angle, M. R., and A. T. Schaefer. 2012. Neuronal recordings with solid-conductor intracellular nanoelectrodes (SCINEs). *PLoS ONE.* 7:e43194.
14. Duan, X., R. Gao, …, C. M. Lieber. 2012. Intracellular recordings of action potentials by an extracellular nanoscale field-effect transistor. *Nat. Nanotechnol.* 7:174–179.
15. Ferguson, J. E., C. Boldt, …, A. D. Redish. 2012. Nanowires precisely grown on the ends of microwire electrodes permit the recording of intracellular action potentials within deeper neural structures. *Nanomedicine (Lond).* 7:847–853.
16. Qing, Q., Z. Jiang, …, C. M. Lieber. 2014. Free-standing kinked nanowire transistor probes for targeted intracellular recording in three dimensions. *Nat. Nanotechnol.* 9:142–147.
17. Robinson, J. T., M. Jorgolli, …, H. Park. 2012. Vertical nanowire electrode arrays as a scalable platform for intracellular interfacing to neuronal circuits. *Nat. Nanotechnol.* 7:180–184.
18. Schrlau, M. G., N. J. Dun, and H. H. Bau. 2009. Cell electrophysiology with carbon nanopipettes. *ACS Nano.* 3:563–568.
19. Tian, B., T. Cohen-Karni, …, C. M. Lieber. 2010. Three-dimensional, flexible nanoscale field-effect transistors as localized bioprobes. *Science.* 329:830–834.
20. Xie, C., Z. Lin, …, B. Cui. 2012. Intracellular recording of action potentials by nanopillar electroporation. *Nat. Nanotechnol.* 7:185–190.
21. Lin, Z. C., X. Chong, …, C. Bianxiao. 2014. Iridium oxide nanotube electrodes for sensitive and prolonged intracellular measurement of action potentials. *Nat. Commun.* 5:3206.
22. Yoon, I., K. Hamaguchi, …, B. R. Donald. 2013. Intracellular neural recording with pure carbon nanotube probes. *PLoS ONE.* 8:e65715.
23. Xie, X., A. M. Xu, …, N. A. Melosh. 2013. Mechanical model of vertical nanowire cell penetration. *Nano Lett.* 13:6002–6008.
24. Guillaume-Gentil, O., E. Potthoff, …, J. A. Vorholt. 2013. Force-controlled fluidic injection into single cell nuclei. *Small.* 9:1904–1907.
25. Reccius, C. H., and P. Fromherz. 2004. Giant lipid vesicles impaled with glass microelectrodes: GigaOhm seal by membrane spreading. *Langmuir.* 20:11175–11182.
26. Almquist, B. D., and N. A. Melosh. 2010. Fusion of biomimetic stealth probes into lipid bilayer cores. *Proc. Natl. Acad. Sci. USA.* 107:5815–5820.
27. Almquist, B. D., and N. A. Melosh. 2011. Molecular structure influences the stability of membrane penetrating biointerfaces. *Nano Lett.* 11:2066–2070.
28. Almquist, B. D., P. Verma, …, N. A. Melosh. 2011. Nanoscale patterning controls inorganic-membrane interface structure. *Nanoscale.* 3:391–400.
29. Hategan, A., R. Law, …, D. E. Discher. 2003. Adhesively-tensed cell membranes: lysis kinetics and atomic force microscopy probing. *Biophys. J.* 85:2746–2759.
30. Bozzola, J. J., and L. D. Russell. 1999. Electron Microscopy: Principles and Techniques for Biologists. Jones & Bartlett Learning, Sudbury, MA.
31. Mollenhauer, H. H. 1993. Artifacts caused by dehydration and epoxy embedding in transmission electron microscopy. *Microsc. Res. Tech.* 26:496–512.
32. Lamers, E., X. F. Walboomers, …, J. A. Jansen. 2010. Cryo dualbeam focused ion beam-scanning electron microscopy to evaluate the interface between cells and nanopatterned scaffolds. *Tissue Eng. Part C Methods.*: August 11. [Epub ahead of print].
33. Hai, A., J. Shappir, and M. E. Spira. 2010. Long-term, multisite, parallel, in-cell recording and stimulation by an array of extracellular microelectrodes. *J. Neurophysiol.* 104:559–568.
34. Hai, A., J. Shappir, and M. E. Spira. 2010. In-cell recordings by extracellular microelectrodes. *Nat. Methods.* 7:200–202.
35. Mason, M. J., A. K. Simpson, …, H. P. C. Robinson. 2005. The interpretation of current-clamp recordings in the cell-attached patch-clamp configuration. *Biophys. J.* 88:739–750.
36. Butt, H.-J., B. Cappella, and M. Kappl. 2005. Force measurements with the atomic force microscope: technique, interpretation and applications. *Surf. Sci. Rep.* 59:1–152.
37. Abdulreda, M. H., and V. T. Moy. 2007. Atomic force microscope studies of the fusion of floating lipid bilayers. *Biophys. J.* 92:4369–4378.

38. Garcia-Manyes, S., G. Oncins, and F. Sanz. 2005. Effect of temperature on the nanomechanics of lipid bilayers studied by force spectroscopy. *Biophys. J.* 89:4261–4274.

39. Künneke, S., D. Krüger, and A. Janshoff. 2004. Scrutiny of the failure of lipid membranes as a function of headgroups, chain length, and lamellarity measured by scanning force microscopy. *Biophys. J.* 86:1545–1553.

40. Loi, S., G. Sun, …, H.-J. Butt. 2002. Rupture of molecular thin films observed in atomic force microscopy. II. Experiment. *Phys. Rev. E Stat. Nonlin. Soft Matter Phys.* 66:031602.

41. Pera, I., R. Stark, …, F. Benfenati. 2004. Using the atomic force microscope to study the interaction between two solid supported lipid bilayers and the influence of synapsin I. *Biophys. J.* 87:2446–2455.

42. Richter, R. P., and A. Brisson. 2003. Characterization of lipid bilayers and protein assemblies supported on rough surfaces by atomic force microscopy†. *Langmuir.* 19:1632–1640.

43. Schneider, J., W. Barger, and G. U. Lee. 2003. Nanometer scale surface properties of supported lipid bilayers measured with hydrophobic and hydrophilic atomic force microscope probes. *Langmuir.* 19:1899–1907.

44. Schneider, J., Y. F. Dufrêne, …, G. U. Lee. 2000. Atomic force microscope image contrast mechanisms on supported lipid bilayers. *Biophys. J.* 79:1107–1118.

45. Butt, H.-J., and V. Franz. 2002. Rupture of molecular thin films observed in atomic force microscopy. I. Theory. *Phys. Rev. E Stat. Nonlin. Soft Matter Phys.* 66:031601.

46. Sen, S., S. Subramanian, and D. E. Discher. 2005. Indentation and adhesive probing of a cell membrane with AFM: theoretical model and experiments. *Biophys. J.* 89:3203–3213.

47. Vakarelski, I. U., S. C. Brown, …, B. M. Moudgil. 2007. Penetration of living cell membranes with fortified carbon nanotube tips. *Langmuir.* 23:10893–10896.

48. Schäfer, A., T. Salditt, and M. C. Rheinstädter. 2008. Atomic force microscopy study of thick lamellar stacks of phospholipid bilayers. *Phys. Rev. E Stat. Nonlin. Soft Matter Phys.* 77:021905.

49. Cruz, J., M. Mihailescu, …, K. Hristova. 2013. A membrane-translocating peptide penetrates into bilayers without significant bilayer perturbations. *Biophys. J.* 104:2419–2428.

50. Derossi, D., A. H. Joliot, …, A. Prochiantz. 1994. The third helix of the Antennapedia homeodomain translocates through biological membranes. *J. Biol. Chem.* 269:10444–10450.

51. Fawell, S., J. Seery, …, J. Barsoum. 1994. Tat-mediated delivery of heterologous proteins into cells. *Proc. Natl. Acad. Sci. USA.* 91:664–668.

52. Oehlke, J., A. Scheller, …, M. Bienert. 1998. Cellular uptake of an α-helical amphipathic model peptide with the potential to deliver polar compounds into the cell interior non-endocytically. *Biochim. Biophys. Acta.* 1414:127–139.

53. Lear, J. D., Z. R. Wasserman, and W. F. DeGrado. 1988. Synthetic amphiphilic peptide models for protein ion channels. *Science.* 240:1177–1181.

54. Sessa, G., J. H. Freer, …, G. Weissmann. 1969. Interaction of alytic polypeptide, melittin, with lipid membrane systems. *J. Biol. Chem.* 244:3575–3582.

55. Lin, M. C., T. Mirzabekov, and B. L. Kagan. 1997. Channel formation by a neurotoxic prion protein fragment. *J. Biol. Chem.* 272:44–47.

56. Cleveland, J. P., S. Manne, …, P. K. Hansma. 1993. A nondestructive method for determining the spring constant of cantilevers for scanning force microscopy. *Rev. Sci. Instrum.* 64:403–405.

57. Conover, W. J. 1980. Practical Nonparametric Statistics. Wiley, New York.

58. de Jesus, A. J., and T. W. Allen. 2013. The role of tryptophan side chains in membrane protein anchoring and hydrophobic mismatch. *Biochim. Biophys. Acta.* 1828:864–876.

59. Andre, G., R. Brasseur, and Y. F. Dufrêne. 2007. Probing the interaction forces between hydrophobic peptides and supported lipid bilayers using AFM. *J. Mol. Recognit.* 20:538–545.

Penetration of Cell Membranes and Synthetic Lipid Bilayers by Nanoprobes

Matthew R. Angle,[1,2] Andrew Wang,[1] Aman Thomas,[1] Andreas T. Schaefer,[2] and Nicholas A. Melosh[1,*]

[1]Department of Materials Science and Engineering, Stanford University, Stanford, California; and [‡]Behavioural Neurophysiology, Max Planck Institute for Medical Research, Heidelberg, Germany

Supporting Material:

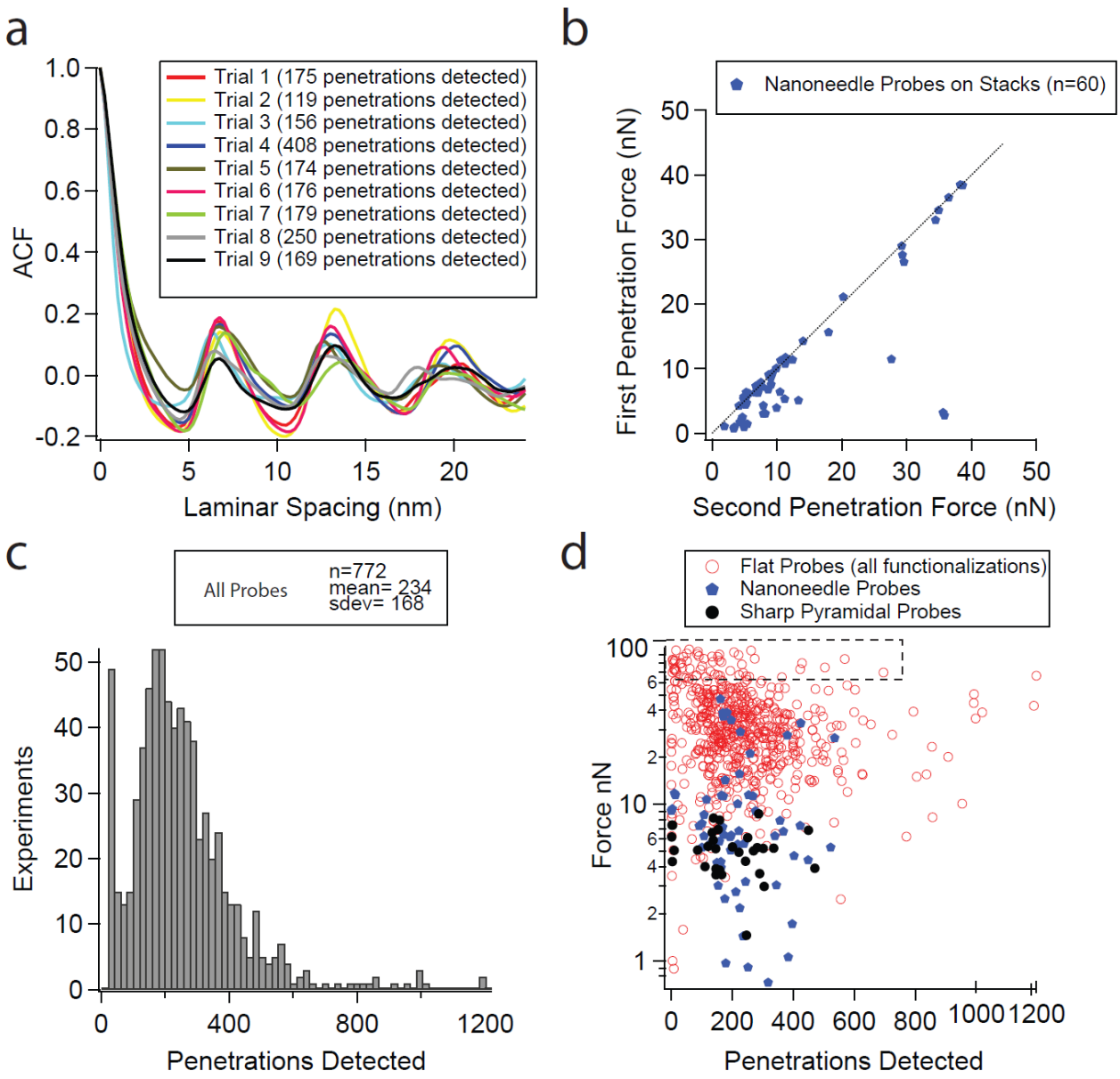

Supplementary Figure 1: On Lipid Stacks

a) Autocorrelation function for the tip position over time. Shows regular, laminar spacing between 6-7 nm. These 9 trials are representative of the entire dataset and were drawn from the nanoneedle experiments.
b) Comparison of first and second breakthrough forces for all experiments performed in lipid stacks using nanoneedle probes. Second breakthrough forces were not analyzed for the other sets of experiments.
c) Histogram of the number of penetrations detected in each lipid stack experiment for all lipid stack experiments (all probe types).
d) Plot of penetration force versus number of penetrations. The variation in thickness has no obvious effect on penetration force. The boxed region indicates where the penetration force is very high. Some of these points may be underestimating the true thickness of the stack if the end-trigger ~100 nN was reached prior to complete penetration of the stack. This shouldn't appreciably effect our conclusion that the stacks are ~200 bilayers thick.

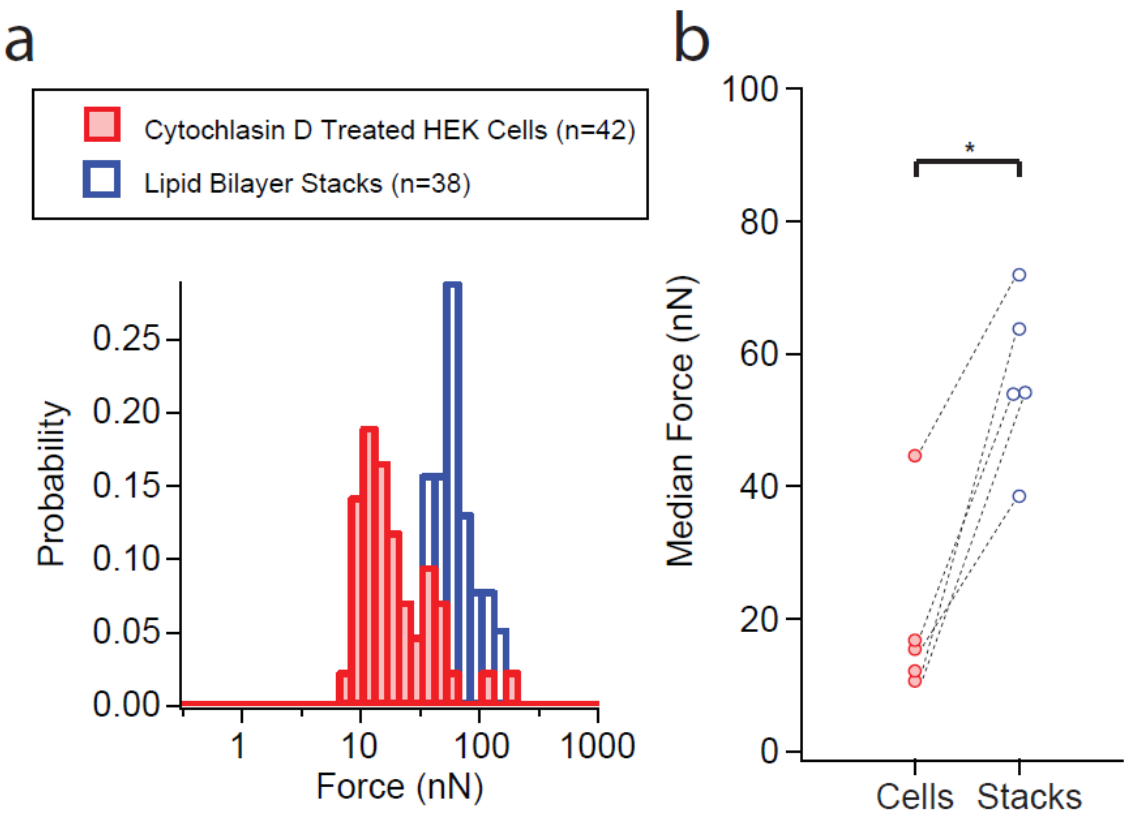

Supplementary Figure 2: Synthetic Oligonucleotide
From a total of 5 functionalized tips.
(*a*) Histogram of all first penetration force in cells and lipid stacks.
(*b*) Pairwise Comparison of median penetration force in cells and lipid stacks for each tip. *Paired T-test P< 0.005.

Supporting Table:

The following table explains the details of the 18 functionalization reagents. It has been split onto two pages and color-coded for display in the merged document. Several of the cell-penetrating peptides were co-functionalized with mercaptopropanol as a competitor (see Concentration). The competitor concentration was based on titration experiments measuring the height of the nitrogen peak from x-ray photoelectron spectroscopy. Concentrations were chosen such that peptide density was non-saturating but > 50%. The rationale for this was to prevent overpacking and steric hindrance. All references in the Supporting Table (1-9) appear elsewhere in the main text.

Supplementary Table 1. Functionalization Reagents for Modifying AFM Tip Surface Chemistry.

Type	Reagent	Sequence	Source	Rationale/Description	Concentration
Peptide	PrPsegement	KTNMKHMAGAAAAGAVVGGLGGRSRGC	Lin et al 1997 [1]	Membrane-inserting (Lin et al 1997) [1]	0.1 mg/mL
	TMD_AR	LSVLRRAVQYLRSLRGSGC	(NP_758513)	Homology to motiff found by Cruz et al 2013 [3]	0.1 mg/mL
	TMD_VTP	LLRGGPACGRLLRGSGC	(NP_080282)	Homology to motiff found by Cruz et al 2013 [3]	0.1 mg/mL
	TMD_Kchan	LLRAGKLRLLRGPGSGC	(NP_001177302)	Homology to motiff found by Cruz et al 2013 [3]	0.1 mg/mL
	Melittin	GIGAVLKVLTTGLPALISWIKRKRQQGSGSGGC	Pubchem CID 16133648	Membrane-inserting (Sessa 1969) [4]	0.1 mg/mL Melittin with 150 µM mercaptopropanol
	TAT	CGGGRKKRRQRRR	PM_12417587	Known CPP (Fawell 1994) [5	0.1 mg/mL TAT with 1 mM mercaptopropanol
	Penetratin	CGGGRQIKIWFQNRRMKWKK	PM_16476052	Known CPP (Derossi et al 1994) 6]	0.1 mg/mL Penetratin with 2 µM mercaptopropanol
	MAP	CGGGKLALKLALKALKAALKLA	PM_10323198	Known CPP (Oehlke et al 1998) [7]	0.1 mg/mL MAP with 10 µM mercaptopropanol
	Lear	LSSLLSLLSSLLSLLSSLLSLGSGC	Lear et al 1988 [2]	Membrane-inserting (Lear et al 1988) [2]	0.1 mg/mL Lear with 1 µM mercaptopropanol
	Propincher	AGRWPPPPPPPWRRRRGSGGSGC		Hydrophobic mismatch (de Jesus 2013) [8]	0.1 mg/mL
	Flexpincher	AGRWLALALALALAWRRRRGSGGSGC		Hydrophobic mismatch (de Jesus 2013) [8]	0.1 mg/mL
	PolyArginine	RRRC		Interaction with phospholipids	0.1 mg/mL PolyArginine with 50 µM mercaptopropanol

Type	Reagent	Sequence	Source	Rationale/Description	Concentration
Nucleotide	DNP-PEG-SPRM	XXXWYWYWY (see Description)	Designed by M. Angle	Amphipathic Oligomer X=DTPA (GlenRes10-1937-xx) Y=DNP (GlenRes 10-1985-xx) W=Spermine (GlenRes 10-1939-xx) From Stanford Pan Oligo (nucleotides from GlenRes)	est. 200 µM

Type	Reagent	Source	Rationale/Description	Concentration
Small molecule	Mercaptopropanol (CAS 19721-22-3)	Sigma	Hydrophillic	100 µM mercaptopropanol
	Dodecanethiol (CAS 112-55-0)	Sigma	Hydrophobic	100 µM 1-decanethiol
	Perfluordecanethiol (CAS 34143-74-3)	Sigma	Very Hydrophobic	100 µM perfluorodecanethiol
	Phenylethanethiol (CAS 4410-99-5)	Sigma	Aromatic	100 µM phenylethanethiol
	Benzophenonethiol	Synthesized by Herbert Zimmerman (MPImF, Heidelberg)	Thiol analog of silane from Angle and Schaefer 2012 [9]	100 µM benzophenonethiol

Supporting References:

1. Lin, M. C., T. Mirzabekov, and B. L. Kagan. 1997. Channel formation by a neurotoxic prion protein fragment. *The Journal of biological chemistry* 272:44-47.
2. Lear, J., Z. Wasserman, and W. DeGrado. 1988. Synthetic amphiphilic peptide models for protein ion channels. *Science* 240:1177-1181.
3. Cruz, J., M. Mihailescu, G. Wiedman, K. Herman, P. C. Searson, W. C. Wimley, and K. Hristova. 2013. A membrane-translocating peptide penetrates into bilayers without significant bilayer perturbations. *Biophys J* 104:2419-2428.
4. Sessa, G., J. H. Freer, G. Colacicco, and G. Weissmann. 1969. Interaction of a Lytic Polypeptide, Melittin, with Lipid Membrane Systems. *Journal of Biological Chemistry* 244:3575-3582.
5. Fawell, S., J. Seery, Y. Daikh, C. Moore, L. L. Chen, B. Pepinsky, and J. Barsoum. 1994. Tat-mediated delivery of heterologous proteins into cells. *Proceedings of the National Academy of Sciences* 91:664-668.
6. Derossi, D., A. H. Joliot, G. Chassaing, and A. Prochiantz. 1994. The third helix of the Antennapedia homeodomain translocates through biological membranes. *Journal of Biological Chemistry* 269:10444-10450.
7. Oehlke, J., A. Scheller, B. Wiesner, E. Krause, M. Beyermann, E. Klauschenz, M. Melzig, and M. Bienert. 1998. Cellular uptake of an α-helical amphipathic model peptide with the potential to deliver polar compounds into the cell interior non-endocytically. *Biochimica et Biophysica Acta (BBA) - Biomembranes* 1414:127-139.
8. de Jesus, A. J., and T. W. Allen. 2013. The role of tryptophan side chains in membrane protein anchoring and hydrophobic mismatch. *Biochimica et biophysica acta* 1828:864-876.
9. Angle, M. R., and A. T. Schaefer. 2012. Neuronal recordings with solid-conductor intracellular nanoelectrodes (SCINEs). *PLoS ONE* 7.